

Article

Comparative Study between Pristine Ag and Ag Foam for Electrochemical Synthesis of Syngas with Carbon Dioxide and Water

Yan Yu, Na Zhong, Jinhui Fang, Shasha Tang, Xincheng Ye, Zhiqiao He and Shuang Song * 

College of Environmental, Zhejiang University of Technology, Hangzhou 310032, China; yanyu1030zx@foxmail.com (Y.Y.); JunoZHONGNa@163.com (N.Z.); jinhuifang1113@163.com (J.F.); TangShasha97@163.com (S.T.); ye_0122xc@163.com (X.Y.); zqhe@zjut.edu.cn (Z.H.)

* Correspondence: ss@zjut.edu.cn; Tel.: +86-571-8832-0726; Fax: 86-571-8832-0276

Received: 14 December 2018; Accepted: 3 January 2019; Published: 8 January 2019



Abstract: The electrosynthesis of syngas ($H_2 + CO$) from CO_2 and H_2O can reduce greenhouse gas emissions and address the energy crisis. In the present work, silver (Ag) foam was employed as a catalytic electrode for the electrochemical reduction of CO_2 in aqueous solution to design different syngas ratios ($H_2:CO$). In addition to H_2 and CO , a small amount of formic acid was found in the liquid phase. By contrast, the planar polycrystalline Ag yields CO , formic acid, methane and methanol as the carbon-containing products. During the potential-controlled electrolysis, the Ag foam displayed a relatively higher activity and selectivity in the electroreduction of aqueous CO_2 to CO compared with its smooth surface counterpart, as evidenced by the lower onset potential, higher partial current density and Faradic efficiency at the same bias voltage. Moreover, the electrode remained stable after three successive cycles. Based on the characterization using X-ray diffraction, field-emission scanning electron microscopy, high-resolution transmission electron microscopy, potential step determination and density functional theory calculations, superior performance was credited to the three-dimensional structure of Ag foam constructed with coral-like Ag particles, in which the numerous edge sites are beneficial for the stabilization of the surface adsorbed $COOH$ species and the exposed $\{111\}$ facets favor the desorption of adsorbed CO species.

Keywords: syngas; Ag foam; carbon dioxide reduction; carbon monoxide; hydrogen

1. Introduction

The exponential increase in anthropogenic carbon dioxide (CO_2) emissions to the Earth's atmosphere, has become one of the most urgent problems for the human society [1,2]. Many feasible methods for decreasing the concentration of CO_2 in the atmosphere have been carried out, such as CO_2 capture, utilization and storage [3–9]. Among these methods, the conversion of CO_2 to useful chemicals with the aid of renewable energy sources (wind, solar, tidal, etc.) plays an important role in addressing current environmental and energy challenges associated with the continued use of fossil fuels [10,11]. However, a major challenge in the implementation of direct renewable energy source-driven CO_2 reduction is the intermittency of energy input, leading to a mismatch between energy supply and demand [12]. Since solar energy, as well as wind and tidal energy, can be stored in the form of electricity, the electrochemical reduction of CO_2 to value-added chemicals is recognized as a potential way to minimize CO_2 emissions and replace fossil fuels [13,14]. In this manner, CO_2 can be transformed to various carbon compounds, including CO , methane, formic acid, alcohols and higher molecular weight hydrocarbons, such as oxalic acid [12,15]. In particular, CO , as a main component of syngas, is an attractive product because of the two-electron reduction process of CO_2 , which seems to provide the best chance for potential industrial application [16,17].

Syngas is a versatile feedstock for producing bulk chemicals and synthetic fuels. The H₂:CO ratio in syngas mixtures can be tuned to 0.6, 0.3–1.0 and 2.0 for Fischer–Tropsch synthesis of hydrocarbons, emerging fermentation and short-chain thermochemical and methanol syntheses, respectively [18]. The co-electrolysis of aqueous CO₂ is desired for large-scale processes and offers a viable alternative to adjust the syngas mixture composition [19].

One bottleneck in the CO₂-water electrochemical reduction to syngas is the preference of the hydrogen evolution reaction (HER). This is because the standard reduction potential for H⁺/H₂O reduction to H₂ at pH 7.0 is −0.41 V versus NHE at pH 7.0, higher than that for CO₂ electroreduction to CO (−0.53 V vs. NHE at pH 7.0) [13,20]. To overcome this limitation, the selection of a suitable electrode that could selectively produce CO seems to be an effective approach for the controllable preparation of syngas. Gold (Au) and silver (Ag) are the two most favorable metal electrodes, with a preference to reduce CO₂ to CO [21]. Compared with Au, Ag is less expensive and thus is considered as a promising metallic material for translating CO₂ into a tunable syngas by varying the electrolyzing potential [22]. Another challenge in the electroreduction of CO₂ is that the reactor should operate at a current density of at least 100 mA cm^{−2}, while still maintaining the CO Faradic efficiency at > 50% [23]. To this end, numerous efforts have been devoted to resolving the mass transfer and reaction kinetics of the electroreduction of CO₂ by improving the electrode, electrolyte and reactor configuration [24,25].

Ag foam is a low density solid with a highly porous structure, providing a large specific area and enabling high permeability. Compared with the flat electrode, the electrons in Ag foam can disperse in a three-dimensional space rather than confined within a two-dimensional space [26]. It is expected that the Ag foam would yield syngas with excellent selectivity at a relatively high current density. Thus, detailed work is required to determine the electroreduction of CO₂ in aqueous solution on Ag foam cathodes.

In the current work, we compare the electrochemical performance of Ag foam and pristine Ag in a CO₂-saturated KHCO₃ solution with a concentration of 0.1 M. The catalytic electrode was characterized using X-ray diffraction (XRD), field-emission scanning electron microscopy (FESEM), transmission electron microscopy (TEM) and potential step determination. The Faradic efficiency (FE), partial current density (PCD) and cyclic use of the electrode were determined via potentiostatic electrolysis. Finally, the possible advantage of Ag foam over pristine Ag was elucidated with the help of density functional theory (DFT) calculations, as well as structural and morphological characterization.

2. Results and Discussion

2.1. Electrode Characterization

2.1.1. XRD

The crystallographic structure of Ag electrodes was investigated by XRD. All the peaks for the Ag foam and pristine Ag were indexed to the cubic phase of Ag (JCPDS card 01-1167). The peaks at 38.1°, 44.37°, 64.18° and 77.55° corresponded to (111), (200), (220) and (311) diffraction planes. No additional obvious characteristic peak was obtained, suggesting the purity of Ag electrodes. Compared with pristine Ag, the relatively sharp peaks of the Ag foam indicate the high crystallinity of the sample (Figure 1). In addition, 2θ values of peak maxima remained unchanged before and after the reaction either for Ag foam or for pristine Ag, suggesting that the crystal structure of the catalyst was sustained during the electro-reduction of CO₂.

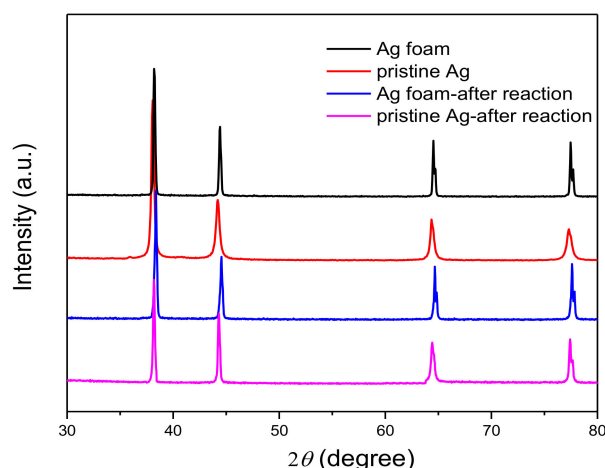


Figure 1. XRD patterns of pristine Ag and Ag foam.

2.1.2. FESEM and High-Resolution TEM (HR-TEM)

The morphology of Ag electrodes was visualized by FESEM. Figure 2a displayed the image of pristine Ag with a rather flat surface and no special morphology. By contrast, a cross-linked grid structure was observed for the Ag foam, as shown in Figure 2b. Furthermore, the typical high magnification scanning electron microscopy (SEM) image of the inset of Figure 2b showed that the Ag foam was constructed of coral-like Ag particles with a particle size of 3–15 μm . Furthermore, it can be observed that the morphology of pristine Ag and Ag foam (Figure 2(a',b')) remained unchanged after the reaction, indicating that the electrodes exhibit excellent structural stability.

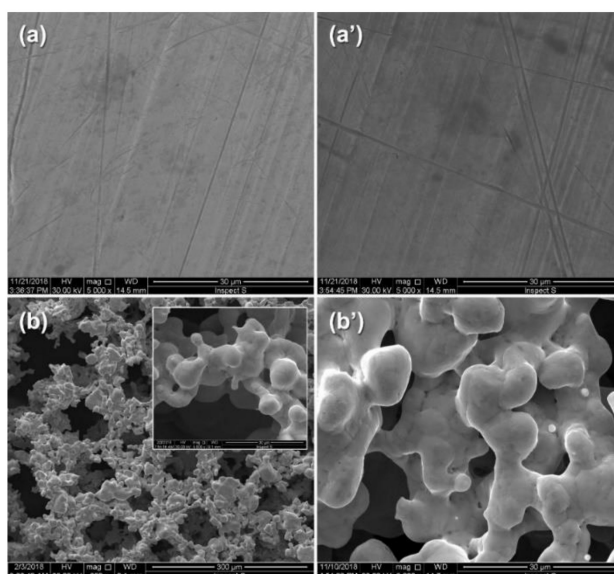


Figure 2. FESEM images of pristine Ag (a), pristine Ag-after reaction (a'), Ag foam (b) and Ag foam-after reaction (b').

To gain a deeper understanding, Ag foam and pristine Ag were further analyzed using HR-TEM. As depicted in Figure 3a, the measured d spacing of 0.24 nm in the HR-TEM image corresponds to the (111) plane of Ag and no other lattice fringes were measured [27,28], indicating that the Ag foam was completely bound by {111} facets. Contrarily, in addition to (111) facet, the d-spacing of 0.21 and 0.15 nm in the pristine Ag can be observed in Figure 3b, corresponding to the (100) and (110) facet, respectively. In other words, the surface of pristine Ag was enclosed by a mix of {111}, {100} and {110} facets. It is worthwhile noting that no obvious change in exposed facet was found for the fresh and

spent electrodes. These results demonstrated that the facet restructure induced by the electro-reduction process hardly occurred.

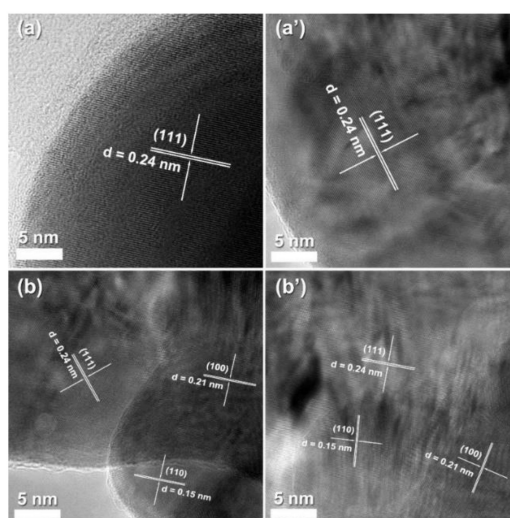


Figure 3. HR-TEM images of Ag foam (a), Ag foam -after reaction (a'), pristine Ag (b) and pristine Ag -after reaction (b').

2.1.3. Roughness Factor and Uncompensated Solution Resistance

The electrochemical area of the electrodes was evaluated by calculating the roughness factor. The roughness factor values for pristine Ag and Ag foam were calculated to be 33.4 and 44.5 $\text{cm}^2 \text{cm}^{-2}$, respectively. Obviously, the former is slightly less than the latter. It should be noted that the pore size at the range of <2.0 nm (micropores) and 2–50 nm (mesopores) contribute mostly to the specific surface area of a material. In this work, the Ag foam electrode contained large amount of pores in micrometer level. Therefore, the roughness factor of the Ag foam was not obviously greater than that of pristine Ag.

Figure 4 presents the Nyquist plots of Electrochemical Impedance Spectroscopy (EIS) for the Ag foam and pristine Ag. The R_u of pristine Ag and Ag foam, derived from the fitting with ZView software (version 3.3, Scribner Associates, Southern Pines, NC, USA), was 28.9 and 32.5 ohm, respectively.

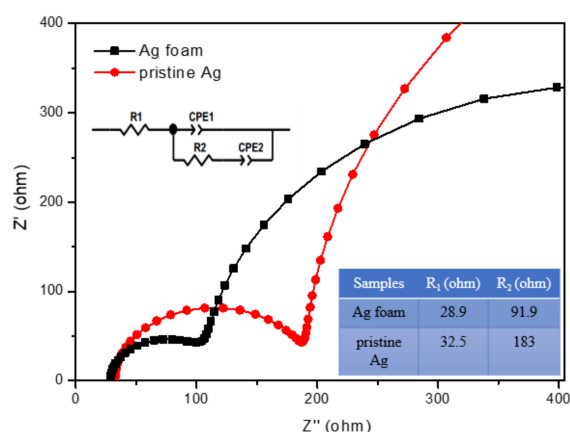


Figure 4. The Nyquist diagrams obtained for Ag foam and pristine Ag. The inset is the equivalent electrical circuit used to fit the EIS data (R_1 denotes the uncompensated electrolyte resistance, CPE1 is the double-layer capacitance at the electrode-electrolyte interface, R_2 is the charge transfer resistance and CPE2 denotes the Warburg-type impedance arising from the diffusion of redox-active species to the electrode interface). Experimental conditions: anolyte, 0.5 M NaOH; catholyte, CO_2 -saturated 0.1 M KHCO_3 ; 25 °C.

2.2. Electrode Selectivity

The applied potential is usually used for controlling the selectivity of an electrochemical reaction. The FE was examined to investigate the effect of applied potential on the overall CO₂ conversion process. A typical variation in FE of CO, methane, formic acid, methanol and H₂ as a function of potential is shown in Figure 5a,b, in which the potentials ranged from −0.53 to −2.97 V for Ag foam and −0.56 to −2.26 V for pristine Ag. It can be seen that Ag foam produces CO and H₂ as major products, accompanied by less solution phase product of formic acid over the entire investigated potential range. Different to pristine Ag, in addition to H₂, CO and formic acid, methane and methanol were accurately detected when the potential was greater than −1.07 and −1.41 V, respectively. During the electroreduction of CO₂ in aqueous solution, the HER inevitably occurred as hydrogen evolution becomes thermodynamically possible at 0 V versus RHE (at any pH) [20,29–31]. Consequently, the HER would compete with the CO₂ reduction at all negative potentials. The evolved H₂ combining with the major product CO became the main composition of so-called syngas [12,15,18,19,22,32–34]. For both electrodes, the total calculated FE of (H₂ + CO) gaseous products was above 90% and other products, such as formic acid, methane and methanol, accounted for no more than 10% of the total FE. In other words, the Ag electrode seems to be a proper alternative for supplying syngas via the electroreduction of aqueous CO₂.

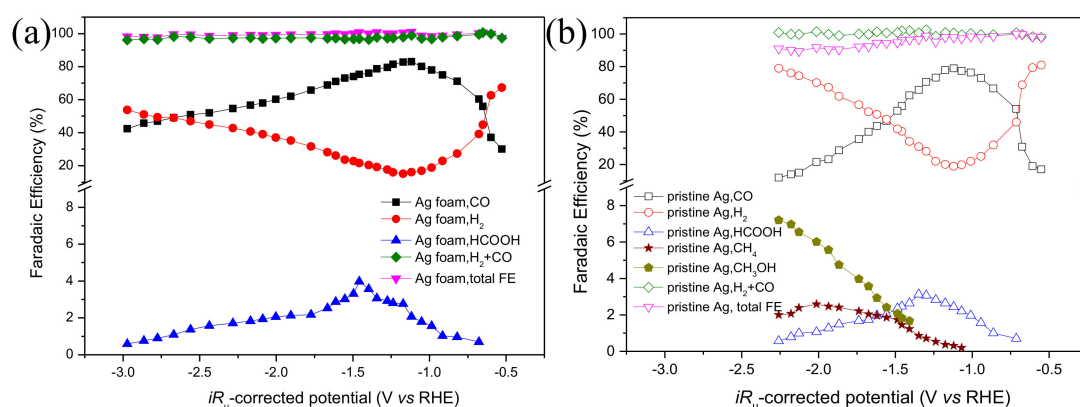


Figure 5. Faradaic efficiency of the CO₂ reduction products for Ag foam (a) and pristine Ag (b) electrodes as a function of electrode potential during the electrolysis process. Experimental conditions: anolyte, 0.5 M NaOH; catholyte, CO₂-saturated 0.1 M KHCO₃; 25 °C.

For Ag foam, CO and formic acid were detected at the starting potentials of −0.53 and −0.68 V, respectively. Methane or methanol was not detected in this work. FE_{CO} and FE_{HCOOH} showed maximum values of 82.9% at −1.12 V and 4.0% at −1.46 V in the potential range of −0.53–−2.97 V. The pristine Ag afforded different onset potentials with respect to Ag foam, which were −0.56 and −0.72 V for CO and formic acid, respectively. The variation in FE_{CO} and FE_{HCOOH} with applied potential exhibited a trend similar to that for Ag foam with maximum values of 79.0% and 3.1% at −1.12 and −1.35 V, respectively. Obviously, the onset potential for the reduction of CO₂ to CO and formic acid on Ag foam shifted ~30 and ~40 mV and was more positive than that on pristine Ag, suggesting that the Ag foam electrode was more active than the polycrystalline Ag electrode.

It should be noted that the onset potential for CO, formic acid, methanol and methane formation on the pristine Ag electrode was at variance with the trend in their redox potentials. The redox potentials of the two-electron reduction of CO₂ to form CO or formic acid, the six-electron reduction of CO₂ to methanol and the eight-electron reduction of CO₂ to methane are −0.53, −0.42, −0.38 and −0.24 V, respectively [22,27,33,35–37]. Therefore, the CO₂ electrochemical reduction reaction was truly under kinetic control compared with thermodynamic control in this study.

Greater differences in the CO₂ reduction selectivity between Ag foam and pristine Ag were observed at the potential window for providing synthetic gas (H₂ + CO). From Figure 6, it can be

seen that an increased H₂ to CO ratio was obtained at more negative potentials. This is because the mass transfer of CO₂ molecules from the bulk solution to the electrode surface dominated the CO₂ electroreduction process with gradually increasing overpotentials, whereas the water reduction to H₂ was rarely mass transfer limited. As an example, if we want to obtain syngas with a H₂:CO ratio of 0.3–1.0 (corresponding to 50.0–76.9% selectivity of CO), the potential ranges would be approximately –0.65––2.77 V and –0.72––1.56 V for Ag foam and pristine Ag, respectively. Obviously, Ag foam afforded a wider potential window than pristine Ag in the electrochemical reduction of aqueous CO₂ to syngas.

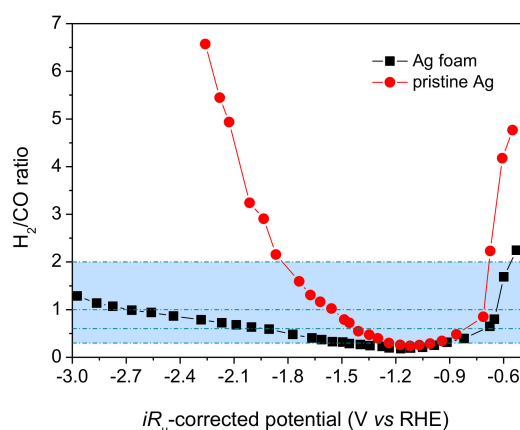
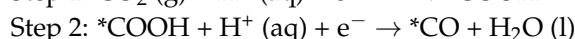
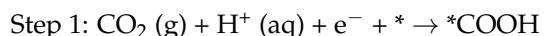


Figure 6. Ratio of H₂:CO in Ag foam and pristine Ag electrodes as a function of electrode potential. Experimental conditions: anolyte, 0.5 M NaOH; catholyte, CO₂-saturated 0.1 M KHCO₃; 25 °C.

The electrochemical reduction of CO₂ on the Ag electrode proceeded via a series of steps as follows:



*COOH and *CO are important intermediates during the reduction of CO₂ [21,22,24,32,38–40]. The binding energy of reaction intermediate plays a vital role in the reaction selectivity [41]. Therefore the binding energy of COOH and CO on different Ag surfaces were calculated and summarized in Table 1. As shown in Table 1, COOH binds the strongest with Ag(100), followed by Ag(110) and Ag(111) surfaces. The strong interaction of COOH on Ag surfaces allowed COOH to stay on the surface and undergo the following reaction steps, which would facilitate the formation of *CO. However, as shown in Table 1, Ag(100) and Ag(110) present strong binding energy of CO among the three Ag surfaces, preventing the desorption of CO from Ag(100) and Ag(110) surface. Different from the case on Ag(110) and Ag(100), once *CO was formed, it would desorb from the Ag(111) surface rapidly due to its weak binding energy on this surface, leading to a higher reaction selectivity on Ag(111).

Table 1. The binding energy of COOH and CO on Ag surfaces.

| Facets | E _{CO} (eV) | E _{COOH} (eV) |
|---------|----------------------|------------------------|
| Ag(111) | –0.15 | –1.15 |
| Ag(110) | –0.33 | –1.44 |
| Ag(100) | –0.35 | –1.62 |

In addition, the number of edge sites and corner sites of Ag is another factor influencing the CO₂ reduction reaction. The catalytic activity of Ag differed significantly with active sites of edge, corner and facet, in the order of edge > corner > facet [21,38,42]. The Ag foam consisted of coral-like particles on the micrometer scale, providing more low-coordinated edge and corner atoms than pristine

Ag for CO₂ electroreduction. This property combined with the positive effect of Ag(111) facets for liberating *CO from the surface resulted in higher selective reduction of CO₂ to syngas by Ag foam than pristine Ag.

2.3. Electrode Activity

The catalytic activity of the electrochemical reduction of CO₂ can be compared by the current density. In Figure 7a,b, the PCD_{CO}, PCD_{H₂}, PCD_{syngas} (PCD_{CO} + PCD_{H₂}) and the total current density are plotted as a function of cathode potential. Obviously, the total current density gradually increased with increasing applied negative potential for pristine Ag and Ag foam electrodes. In addition, Ag foam displayed ~1.2-fold higher total current density compared with pristine Ag in the range investigated.

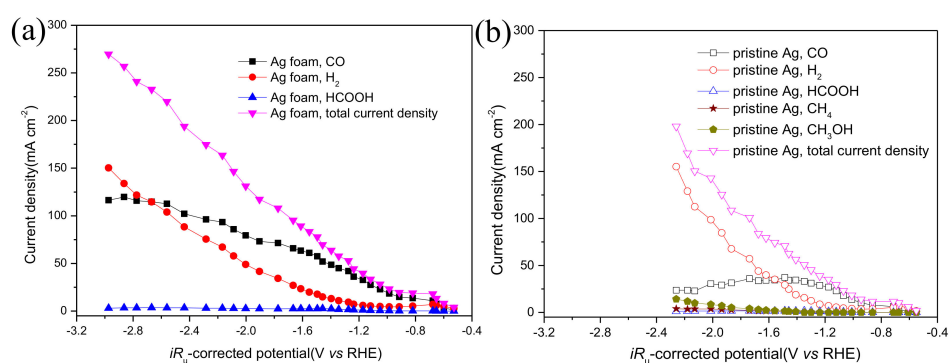


Figure 7. Partial current density of each reduction product for Ag foam (a) and pristine Ag (b) electrodes as a function of potential. Experimental conditions: anolyte, 0.5 M NaOH; catholyte, CO₂-saturated 0.1 M KHCO₃; 25 °C.

At a H₂:CO molar ratio of 0.3–1.0, PCD_{syngas} of pristine Ag and Ag foam showed a similar increasing trend with negatively shifted the electrolysis voltage, as shown in Figure 8. Pristine Ag produced the maximum current density of 69.58 mA cm⁻² at -1.56 V, at the same current density, the potential on the Ag foam cathode was shifted positively by 180 mV. As a consequence, Ag foam displayed an elevated preference for the electroreduction of CO₂ to syngas. It should be noted that the maximum current density of 237.58 mA cm⁻² for PCD_{syngas} production was reached on Ag foam at a potential of -2.77 V, which was ~3.4-fold greater than that observed on pristine Ag (69.58 mA cm⁻² at -1.56 V). Therefore, Ag foam resulted in a much higher current density in the electrochemical reduction of CO₂ to CO and thus seems to be a promising electrode with great potential for industrial applications.

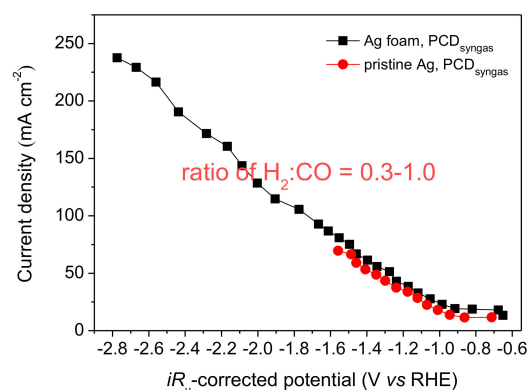


Figure 8. Current density of syngas at the ratio of 0.3–1.0 H₂:CO for Ag foam and pristine Ag electrodes as a function of potential. Experimental conditions: anolyte, 0.5 M NaOH; catholyte, CO₂-saturated 0.1 M KHCO₃; 25 °C.

To exclude the influence of surface area, the values of the PCD per unit of electrochemical surface area of electrode were calculated and the results are shown in Table 2 and Figure 9. As one of the components of syngas, CO was produced on Ag foam with a SA greater than that on pristine Ag. Consequently, the intrinsic properties other than surface area, such as exposed crystal faces, edges and corner sites, contributed to the improved activity of the electroreduction of CO₂ to CO.

Table 2. The specific activity for the formation of CO on Ag foam and pristine Ag.

| Sample | Roughness Factor (cm ² cm ⁻²) | Potential (V vs. RHE) | PCD _{CO} (mA cm ⁻²) | SA _{CO} (10 ⁻⁵ A cm ⁻²) |
|-------------|------------------------------------------------------|-----------------------|------------------------------------------|---------------------------------------------------------|
| Ag foam | 44.5 | -0.53 | 1.20 | 2.70 |
| | | -0.60 | 2.97 | 6.68 |
| | | -0.65 | 7.38 | 16.59 |
| pristine Ag | 33.4 | -0.56 | 0.34 | 1.02 |
| | | -0.61 | 1.15 | 3.46 |
| | | -0.68 | 3.11 | 9.32 |

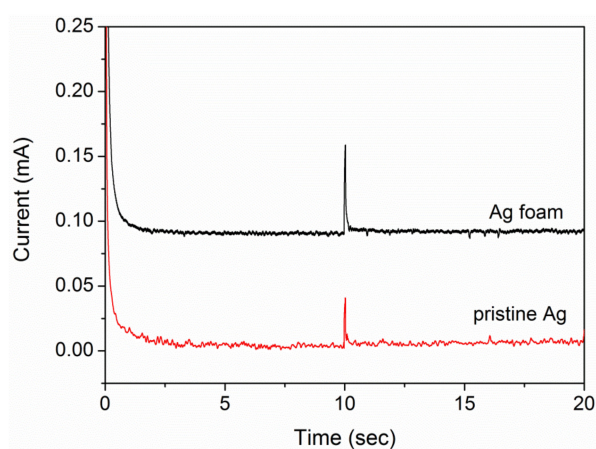


Figure 9. Potential-step curves of the Ag foam and pristine Ag electrodes.

As discussed previously, Ag(111) is a suitable electrocatalyst for stabilizing *COOH and liberating *CO. Furthermore, the edge sites of Ag would enhance the activation of CO₂ to *COOH. Consequently, the Ag foam electrode with fully exposed {111} facets and more edge sites, in comparison with polycrystalline pristine Ag electrode, quickly reduced CO₂ to *COOH and *CO and released *CO from the electrode surface in the form of CO. A comparison of the activity and selectivity achieved with these Ag electrocatalysts with previous references is provided in Table 3. It demonstrated that the performance of Ag foam have a superior activity and comparable selectivity of CO production to similar reported materials [7,27,30,39,42,43]. In other words, the Ag foam afforded a higher PCD_{syngas} than pristine Ag in the aqueous electrochemical reduction of CO₂.

Table 3. The comparison of the activity and selectivity with different Ag electrodes.

| Morphology of Ag Electrodes | Electrolyte | Selective Production of CO | | | Ref. |
|---------------------------------|-------------------------|-------------------------------|-------------------------|----------------------------------------|-------------|
| | | Applied Potential V (vs. RHE) | Faradaic Efficiency (%) | Current Density (mA cm ⁻²) | |
| Nanoparticles | 0.5 M KHCO ₃ | -0.75 | 79 | 1 | 43 |
| Nanoporous | 0.5 M KHCO ₃ | -0.60 | 92 | 18 | 30 |
| Nanocorals | 0.1 M KHCO ₃ | -0.60 | 95 | 6.62 | 39 |
| Oxide-derived | 0.1 M KHCO ₃ | -0.80 | 89 | 1.15 | 44 |
| Compact grains | 0.1 M KHCO ₃ | -1.1 | 88.87 | 5.73 | 7 |
| Truncated hexagonal bipyramidal | 0.1 M KHCO ₃ | -0.93 | 89.4 | 4.92 | 27 |
| Plate | 0.1 M KHCO ₃ | -1.12 | 79.0 | 22.93 | In our work |
| Foam | 0.1 M KHCO ₃ | -1.12 | 82.9 | 27.43 | In our work |

2.4. Electrode Stability

The stability of an electrode is a critical challenge in commercial applications. Taking the first applied potential with the syngas $H_2:CO$ molar ratio of 1 as an example, the variation in FE_{CO} and FE_{H_2} as a function of time are plotted in Figure 10. During the 4-h reaction period, the variation in FE_{CO} and FE_{H_2} on Ag foam compared with pristine Ag showed a different tendency. For Ag foam, the FE_{CO} rapidly increased to the maximum value of 56.94% in the first 30 min of electrolysis and then slowly weakened to 54.96% in the next reaction period. By contrast, the FE_{CO} reached the maximum value of 54.39% at 60 min and promptly dropped to 39.78% at the end of the reaction with pristine Ag. The slight decrease in FE_{CO} with the Ag foam electrode may have been due to the mass transfer limitation of CO_2 in the batch experiment, as seen previously [9,20,23,24,35]. Different to Ag foam, we believe that the striking decrease in FE_{CO} on pristine Ag stemmed from a poisoning effect rather than the limitation of mass transfer.

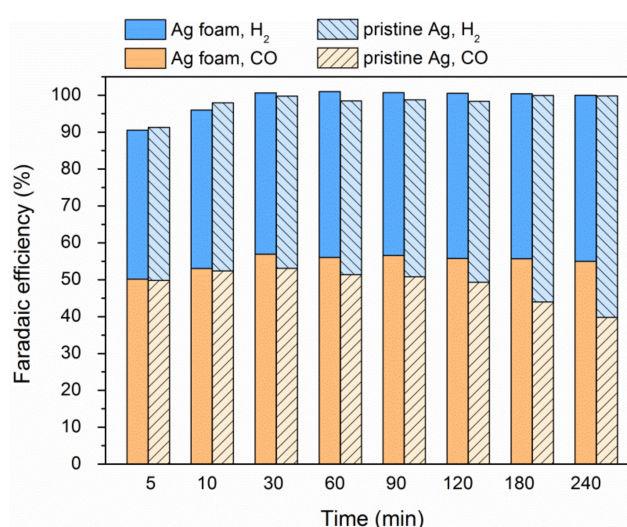


Figure 10. Faradic efficiency of CO and H_2 at different time intervals during polarization at -0.65 and -0.72 V with $H_2:CO = 1$ for Ag foam and pristine Ag, respectively. Experimental conditions: anolyte, 0.5 M NaOH; catholyte, CO_2 -saturated 0.1 M $KHCO_3$; 25 °C.

The Ag foam had a higher PCD_{CO} at -0.65 V (7.38 mA cm^{-2}) than pristine Ag at -0.72 V (6.23 mA cm^{-2}). Thus, Ag foam consumed more soluble CO_2 in the catholyte than pristine Ag. Theoretically, the concentration decrease in CO and the corresponding concentration increase in H_2 on pristine Ag should be slower than those on the Ag foam electrode. Nonetheless, the curves in Figure 10 clearly display the opposite trend.

As shown in previous studies, the overbinding of $*CO$ and/or protonated $*CO$ can lead to surface poisoning of the Ag electrode [20,44,45]. It is well known that the stability of adsorbed species is closely related to the exposed facets of the crystals, which directly affect the properties of the catalysts. As previously mentioned, the binding energy of CO for different crystal planes of Ag follows the order: $Ag(110) > Ag(100) > Ag(111)$. Therefore, $*CO$ was desorbed more easily on $Ag(111)$ than on $Ag(110)$. Thus, relative to pristine Ag enclosed with mixed (111), (110) and (100) facets, Ag foam with only a single exposed facet of (111) could maintain its activity and prolong the electrolysis time.

To further elucidate the high stability of the Ag foam electrode, we performed recycling experiments at a high potential of -2.67 V, where the molar ratio of H_2 to CO was ~ 1 . As displayed in Figure 11, no obvious difference in the variation of FE_{CO} and FE_{H_2} was observed for Ag foam over three runs of electrochemical reduction of CO_2 . After each run, FE_{CO} returned to its original activity upon resaturation of the catholyte with CO_2 . The results of the time-dependent experiments confirmed that the Ag foam was not deactivated during the course of electroreduction of CO_2 in aqueous solution.

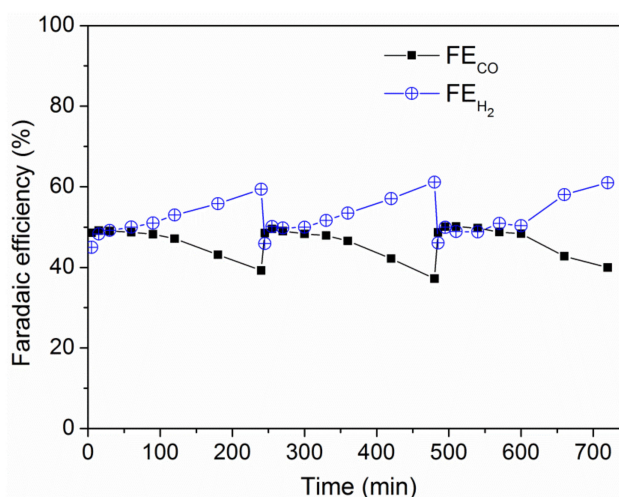


Figure 11. Cyclic yield curve of CO and H₂ on Ag foam electrode from re-saturated used electrolyte at -2.67 V. Experimental conditions: anolyte, 0.5 M NaOH; catholyte, CO₂-saturated 0.1 M KHCO₃; 25 °C.

3. Experimental

3.1. Materials and Reagents

Ag foam and pristine Ag (99.99% purity) were purchased from Kunshan Jiayisheng Electronics Co., Ltd., Kunshan, China and Jinjiang Dongyin Jewelry Co., Ltd., Jinjiang, China, respectively. CO₂ (purity 99.995%), CO (purity 99.99%), H₂ (purity 99.999%) and methane (purity 99.99%) were provided by Hangzhou Jingong Special Gas Co., Ltd., Hangzhou, China. All the reagents used in the present study, including NaOH, KHCO₃, KCl, acetone and ethanol, were of analytical grade and were obtained from Huadong Medical Co., Ltd., Hangzhou, China. Milli-Q water (18.2 MΩ) was used in all experiments.

3.2. Electrode Characterization

XRD patterns were recorded by a PANalytical X'Pert Pro X-ray diffractometer using Cu Kα radiation ($k = 1.5406$ Å) with a scan step of 0.05° between 10° and 80° . FESEM was performed on a Hitachi S-4800 operating at an accelerating voltage of 5 kV. TEM and high-resolution TEM (HR-TEM) images were observed with a Philips-FEI Tecnai G2 F30 S-Twin microscope with an accelerating voltage of 300 kV.

The surface roughness of the electrodes was obtained by calculating the roughness factor (ρ) according to Equation (1).

$$\rho = \frac{\int_0^t (I - I_\infty) dt}{\Delta\phi \times C \times S} \quad (1)$$

where I and I_∞ denote the current and stable current value after a step, respectively, S is the geometric area of the electrode, which is 0.25 cm^2 ($0.5 \text{ cm} \times 0.5 \text{ cm}$ in length and width) for both pristine Ag and Ag foam and C is equal to $20 \mu\text{F cm}^{-2}$, representing the double-layer capacitance for an ideally smooth electrode. I and I_∞ were obtained by using the multi-potential step mode of an electrochemical workstation (CHI760E, CH Instrument, Bee Cave, TX, USA) in a 0.5 mol L^{-1} NaClO₄ aqueous solution at 20 °C. The potential of the electrodes was held at 0.10 V versus the saturated calomel electrode (SCE) for 10 s and then stepped to 0.095 V versus SCE for 10 s. Consequently, the t and $\Delta\phi$ in Equation (1) were 10 s and 5 mV, respectively.

The uncompensated solution resistance (R_{u}) were determined from EIS measurements. The EIS experiments were conducted in the dark at room temperature, with a frequency range of 1000 kHz to 0.01 Hz and AC amplitude of 0.005 V.

The DFT calculations of E_{CO} and E_{COOH} were performed by the Vienna Ab initio Simulation Package with PW-91 functions in the generalized gradient approximation calculation. A kinetic cutoff energy of 396 eV was used for the plane wave truncation and a periodic $3 \times 3 \times 1$ Monkhorst-Pack k-point grid were used for all calculations. All surfaces were modelled by adding six equivalent layers of vacuum onto four layers of metal atoms corresponding to the most close-packed configurations. The two bottom layers of the slab were fixed, a lattice parameter of 4.09 Å was used for Ag, whereas the top two layers were allowed to relax to reach the lowest energy configuration. The binding energy was calculated using the equation:

$$E_{\text{adsorbate/slab}} = E_{\text{adsorbate/slab}} - E_{\text{slab}} - E_{\text{adsorbate}} \quad (2)$$

where $E_{\text{adsorbate/slab}}$ is the binding energy of adsorbate on the given slab, $E_{\text{adsorbate/slab}}$ is the energy of the surface with adsorbate, E_{slab} is the energy of the slab in vacuum and $E_{\text{adsorbate}}$ is the energy of adsorbate in the gas phase. Different adsorption sites, such as atop, bridge, fcc and hcp, were calculated for CO. E_{COOH} investigated the formate chemisorption in a symmetric bidentate configuration at the bridge on Ag surfaces.

3.3. Electrochemical Reduction of CO_2

All electrochemical reduction experiments were conducted using a three-electrode configuration controlled by a CHI 760E potentiostat. The reactor was a gas-tight two-compartment electrochemical cell with a cation-exchange membrane (Nafion-117) as the separator. Ag foam or pristine Ag (50 mm \times 50 mm \times 0.3 mm) was used as the working electrode, which was cleaned and degreased with acetone, ethanol and Milli-Q water for 1.5 h, washed thoroughly and dried by N_2 . A platinum sheet was employed as the counter electrode. All potentials were measured against the SCE and converted to a reversible hydrogen electrode (RHE) scale based on the Nernst equation. The anolyte and catholyte were 0.5 M NaOH and 0.1 M KHCO_3 with solution saturated with CO_2 (pH 6.8), respectively.

Potential conversion to a RHE scale and iR_u corrections were made to assess the activity and selectivity of the electrode on the same bias, as shown in Equation (3).

$$E = E (\text{vs. SCE}) + 0.2412 \text{ V} + 0.0591 \text{ V} \times \text{pH} - iR_u \quad (3)$$

where E and E (vs. SCE) are the final reported potential and applied potential, respectively, i is the average current and R_u is the uncompensated solution resistance.

The FE value of the electrode catalyst for CO_2 electroreduction was calculated using the following equation:

$$\text{FE} = \frac{z \times n \times F}{Q} \quad (4)$$

where z represents the number of electrons exchanged (z is equal to 2 for the reduction of CO_2 to HCOOH and H_2 , respectively), n is the number of moles of a given product, F is Faraday's constant (96485 C mol^{-1}) and Q is the charge passed (C).

The PCD of productions was calculated from the gas chromatograph (GC) peak area as follows:

$$\text{PCD} = j_{\text{total}} \times \text{FE} = j_{\text{total}} \cdot \frac{z \times n \times F}{Q} \quad (5)$$

where j_{total} is the total current density, n is the molar of productions and Q is the amount of charge passed during the reaction.

3.4. Analytical Procedures

The GC (7890B, Agilent, Santa Clara, CA, USA) was equipped with a HP-MOLESIEVE capillary column (30 m \times 0.32 mm \times 12 mm). Helium (99.999%) was used as the carrier gas. A thermal

conductivity detector was used to quantify the H₂ and CO concentrations. The amount of methane in the gas phase was measured using GC (GC-2014, Shimadzu, Tokyo, Japan) equipped with a flame ionization detector (FID) and an HPPLLOT/Q column (30 m × 0.32 mm × 20 mm). The concentration of methanol volatilized from the liquid phase to the gas phase was quantified by GC (7890B, Agilent, USA) equipped with a FID and an HP-INNOWAX capillary column (30 m × 0.25 mm × 25 mm). The liquid phase product formic acid dissolved in the catholyte was determined using ion chromatography (ICS2000, Dionex, Sunnyvale, CA, USA) equipped with a conductivity detector (DS6, Dionex), a guard column (IonPac AG19, Dionex, Sunnyvale, CA, USA), an analytical column (IonPac AS19, Dionex, Sunnyvale, CA, USA) and a dual-piston (in series) pump. Suppression of the eluent was achieved using a Dionex anion ASRS electrolytic suppressor (4 mm) in the auto-suppression external water mode.

4. Conclusions

We demonstrated that Ag foam is an efficient catalyst for the electrochemical reduction of CO₂ to syngas in aqueous solution. Ag foam was superior to pristine Ag in terms of the onset potential of CO, Faradic efficiency and partial current density of syngas. When producing CO (one of the main components of syngas), Ag foam showed a ~30 mV more positive onset potential than pristine Ag. The FE_{CO} and PCD_{syngas} of Ag foam were maximum at −1.12 and −2.77 V (82.9% and 237.58 mA cm^{−2}, respectively), compared to a maximal FE_{CO} value of 79.0% at −1.12 V and PCD_{syngas} of 69.58 mA cm^{−2} at −1.56 V for pristine Ag, respectively. For the molar ratio of H₂:CO at 0.3–1.0, Ag foam showed a wider potential window of 2.12 V than pristine Ag (0.84 V). In addition, Ag foam displayed fairly stable electrolysis performance in the three cyclic durability tests. DFT calculations demonstrated that the low-index Ag (111) plane favors the desorption of *CO. Furthermore, the edge sites govern the stabilization of *COOH. Namely, the abundant edge sites of coral-like Ag with large number of {111} facets could increase the selectivity, activity and stability of the Ag foam electrode. This Ag foam electrode provides an option for obtaining a flexible ratio of H₂:CO in the production of syngas to meet the requirements of downstream products.

Author Contributions: Conceptualization, S.S.; Data curation, Y.Y. and N.Z.; Formal analysis, J.F. and X.Y.; Software, S.T.; Supervision, Z.H.; Writing—original draft, Y.Y.

Funding: This research received no external funding.

Acknowledgments: This work was supported by the National Science Foundation of China (21477117 and 21607130), the Zhejiang Provincial Natural Science Foundation of China (LZ18B070001, LGF18E080017 and LR14E080001) and the China Postdoctoral Science Foundation (2017T100436).

Conflicts of Interest: The authors declare no conflict of interest.

References

1. Olah, G.A.; Prakash, G.K.S.; Goepfert, A. Anthropogenic chemical carbon cycle for a sustainable future. *J. Am. Chem. Soc.* **2011**, *133*, 12881–12898. [[CrossRef](#)] [[PubMed](#)]
2. Luo, P.P.; Zhang, Y.T.; Chen, B.L.; Yu, S.X.; Zhou, H.W.; Qu, K.G.; Kong, Y.X.; Huang, X.Q.; Zhang, X.X.; Lu, J.X. Electrocarboxylation of dichlorobenzenes on a silver electrode in DMF. *Catalysts* **2017**, *7*, 274. [[CrossRef](#)]
3. Zhang, S.H.; Shen, Y.; Shao, P.J.; Chen, J.M.; Wang, L.D. Kinetics, thermodynamics, and mechanism of a novel biphasic solvent for CO₂ capture from flue gas. *Environ. Sci. Technol.* **2018**, *52*, 3660–3668. [[CrossRef](#)] [[PubMed](#)]
4. Zhao, J.; Ye, J.H.; Zhu, N.; Hong, H.L.; Ma, L.; Yang, J.R.; Zhang, J.B. Amine phase-transfer chemistry: A green and sustainable approach to the nonbiological mineralization of CO₂. *ACS Sustain. Chem. Eng.* **2018**, *6*, 7105–7108. [[CrossRef](#)]
5. Zhang, S.H.; Lu, Y.Q. Surfactants facilitating carbonic anhydrase enzyme-mediated CO₂ absorption into a carbonate solution. *Environ. Sci. Technol.* **2017**, *51*, 8537–8543. [[CrossRef](#)] [[PubMed](#)]
6. Zhang, S.H.; Du, M.E.; Shao, P.J.; Wang, L.D.; Ye, J.X.; Chen, J.; Chen, J.M. Carbonic anhydrase enzyme-MOFs composite with a superior catalytic performance to promote CO₂ absorption into tertiary amine solution. *Environ. Sci. Technol.* **2018**, *52*, 12708–12716. [[CrossRef](#)]

7. Qiu, J.P.; Tang, J.T.; Shen, J.; Wu, C.W.; Qian, M.Q.; He, Z.Q.; Chen, J.M.; Song, S. Preparation of a silver electrode with a three-dimensional surface and its performance in the electrochemical reduction of carbon dioxide. *Electrochim. Acta* **2016**, *203*, 99–108.
8. Wang, J.L.; Zhou, S.Y.; Bei, K.; Zhang, D.; Chou, I.M.; Chen, Z.H.; Lin, C.M.; Pan, Z.Y. Using a fused silica capillary cell and in situ raman spectroscopy to develop a setup for measurement of the volume expansion of carbon dioxide + n-hexane. *Energy Fuel* **2017**, *31*, 6314–6319. [[CrossRef](#)]
9. Ma, L.; Fan, S.; Zhen, D.X.; Wu, X.M.; Liu, S.S.; Lin, J.J.; Huang, S.Q.; Chen, W.; He, G.H. Electrochemical reduction of CO₂ in proton exchange membrane reactor: The function of buffer layer. *Ind. Eng. Chem. Res.* **2017**, *56*, 10242–10250. [[CrossRef](#)]
10. Zhong, H.; Fujii, K.; Nakano, Y.; Jin, F.M. Effect of CO₂ bubbling into aqueous solutions used for electrochemical reduction of CO₂ for energy conversion and storage. *J. Phys. Chem. C* **2014**, *119*, 55–61. [[CrossRef](#)]
11. Yuan, J.; Zhang, J.J.; Yang, M.P.; Meng, W.J.; Wang, H.; Lu, J.X. CuO nanoparticles supported on TiO₂ with high efficiency for CO₂ electrochemical reduction to ethanol. *Catalysts* **2018**, *8*, 171. [[CrossRef](#)]
12. Foit, S.R.; Vinke, I.C.; de Haart, L.G.J.; Eichel, R.A. Power-to-syngas: An enabling technology for the transition of the energy system? *Angew. Chem.-Int. Ed.* **2017**, *56*, 5402–5411. [[CrossRef](#)] [[PubMed](#)]
13. Fu, Y.S.; Li, Y.N.; Zhang, X.; Liu, Y.Y.; Qiao, J.L.; Zhang, J.J.; Wilkinson, D.P. Novel hierarchical SnO₂ microsphere catalyst coated on gas diffusion electrode for enhancing energy efficiency of CO₂ reduction to formate fuel. *Appl. Energy* **2016**, *175*, 536–544. [[CrossRef](#)]
14. Yuan, J.; Liu, L.; Guo, R.R.; Zeng, S.; Wang, H.; Lu, J.X. Electroreduction of CO₂ into ethanol over an active catalyst: Copper supported on titania. *Catalysts* **2017**, *7*, 220. [[CrossRef](#)]
15. Kang, P.; Chen, Z.F.; Nayak, A.; Zhang, S.; Meyer, T.J. Single catalyst electrocatalytic reduction of CO₂ in water to H₂ + CO syngas mixtures with water oxidation to O₂. *Energy Environ. Sci.* **2014**, *7*, 4007–4012. [[CrossRef](#)]
16. Costentin, C.; Drouet, S.; Robert, M.; Saveant, J.M. A local proton source enhances CO₂ electroreduction to CO by a molecular Fe catalyst. *Science* **2012**, *338*, 90–94. [[CrossRef](#)] [[PubMed](#)]
17. Feng, D.M.; Zhu, Y.P.; Chen, P.; Ma, T.Y. Recent advances in transition-metal-mediated electrocatalytic CO₂ reduction: From homogeneous to heterogeneous systems. *Catalysts* **2017**, *7*, 373. [[CrossRef](#)]
18. Ross, M.B.; Dinh, C.T.; Li, Y.; Kim, D.; De Luna, P.; Sargent, E.H.; Yang, P. Tunable Cu enrichment enables designer syngas electrosynthesis from CO₂. *J. Am. Chem. Soc.* **2017**, *139*, 9359–9363. [[CrossRef](#)]
19. Fu, Q.; Mabilat, C.; Zahid, M.; Brisse, A.; Gautier, L. Syngas production via high-temperature steam/CO₂ co-electrolysis: An economic assessment. *Energy Environ. Sci.* **2010**, *3*, 1382. [[CrossRef](#)]
20. Sheng, W.C.; Kattel, S.; Yao, S.Y.; Yan, B.H.; Liang, Z.X.; Hawxhurst, C.J.; Wu, Q.Y.; Chen, J.G.G. Electrochemical reduction of CO₂ to synthesis gas with controlled CO/H₂ ratios. *Energy Environ. Sci.* **2017**, *10*, 1180–1185. [[CrossRef](#)]
21. Back, S.; Yeom, M.S.; Jung, Y. Active sites of Au and Ag nanoparticle catalysts for CO₂ electroreduction to CO. *ACS Catal.* **2015**, *5*, 5089–5096. [[CrossRef](#)]
22. Hernández, S.; Amin Farkhondehfal, M.; Sastre, F.; Makkee, M.; Saracco, G.; Russo, N. Syngas production from electrochemical reduction of CO₂: Current status and prospective implementation. *Green Chem.* **2017**, *19*, 2326–2346. [[CrossRef](#)]
23. Oloman, C.; Li, H. Electrochemical processing of carbon dioxide. *ChemSusChem* **2008**, *1*, 385–391. [[CrossRef](#)]
24. Verma, S.; Hamasaki, Y.; Kim, C.; Huang, W.; Lu, S.; Jhong, H.-R.M.; Gewirth, A.A.; Fujigaya, T.; Nakashima, N.; Kenis, P.J.A. Insights into the low overpotential electroreduction of CO₂ to CO on a supported gold catalyst in an alkaline flow electrolyzer. *ACS Energy Lett.* **2017**, *3*, 193–198. [[CrossRef](#)]
25. Schmid, B.; Reller, C.; Neubauer, S.S.; Fleischer, M.; Dorta, R.; Schmid, G. Reactivity of copper electrodes towards functional groups and small molecules in the context of CO₂ electro-reductions. *Catalysts* **2017**, *7*, 161. [[CrossRef](#)]
26. Costentin, C.; Robert, M.; Savéant, J.-M. Catalysis of the electrochemical reduction of carbon dioxide. *Chem. Soc. Rev.* **2013**, *42*, 2423–2436. [[CrossRef](#)]
27. He, Z.Q.; Liu, T.; Tang, J.T.; Zhou, C.Y.; Wen, L.S.; Chen, J.M.; Song, S. Highly active, selective and stable electroreduction of carbon dioxide to carbon monoxide on a silver catalyst with truncated hexagonal bipyramidal shape. *Electrochim. Acta* **2016**, *222*, 1234–1242. [[CrossRef](#)]

28. Zhang, P.; Shao, C.L.; Zhang, Z.Y.; Zhang, M.Y.; Mu, J.B.; Guo, Z.C.; Liu, Y.C. In situ assembly of well-dispersed Ag nanoparticles (AgNPs) on electrospun carbon nanofibers (CNFs) for catalytic reduction of 4-nitrophenol. *Nanoscale* **2011**, *3*, 3357–3363. [[CrossRef](#)]
29. Peterson, A.A.; Nørskov, J.K. Activity descriptors for CO₂ electroreduction to methane on transition-metal catalysts. *J. Phys. Chem. Lett.* **2012**, *3*, 251–258. [[CrossRef](#)]
30. Lu, Q.; Rosen, J.; Zhou, Y.; Hutchings, G.S.; Kimmel, Y.C.; Chen, J.G.G.; Jiao, F. A selective and efficient electrocatalyst for carbon dioxide reduction. *Nat. Commun.* **2014**, *5*, 3242. [[CrossRef](#)]
31. Gao, D.F.; Zhang, Y.; Zhou, Z.W.; Cai, F.; Zhao, X.F.; Huang, W.G.; Li, Y.S.; Zhu, J.F.; Liu, P.; Yang, F.; et al. Enhancing CO₂ electroreduction with the metal-oxide interface. *J. Am. Chem. Soc.* **2017**, *139*, 5652–5655. [[CrossRef](#)] [[PubMed](#)]
32. Li, W. Electrocatalytic reduction of CO₂ to small organic molecule fuels on metal catalysts. *Cheminform* **2010**, *1056*, 55–76.
33. Zhao, S.; Jin, R.X.; Jin, R.C. Opportunities and challenges in CO₂ reduction by gold- and silver-based electrocatalysts: From bulk metals to nanoparticles and atomically precise nanoclusters. *ACS Energy Lett.* **2018**, *3*, 452–462. [[CrossRef](#)]
34. Kumar, B.; Brian, J.P.; Atla, V.; Kumari, S.; Bertram, K.A.; White, R.T.; Spurgeon, J.M. Controlling the product syngas H₂:CO ratio through pulsed-bias electrochemical reduction of CO₂ on copper. *ACS Catal.* **2016**, *6*, 4739–4745. [[CrossRef](#)]
35. Zhang, W.J.; Hu, Y.; Ma, L.B.; Zhu, G.Y.; Wang, Y.R.; Xue, X.L.; Chen, R.P.; Yang, S.Y.; Jin, Z. Progress and perspective of electrocatalytic CO₂ reduction for renewable carbonaceous fuels and chemicals. *Adv. Sci.* **2018**, *5*, 1700275. [[CrossRef](#)] [[PubMed](#)]
36. Jiang, B.; Zhang, X.G.; Jiang, K.; Wu, D.Y.; Cai, W.B. Boosting formate production in electrocatalytic CO₂ reduction over wide potential window on Pd surfaces. *J. Am. Chem. Soc.* **2018**, *140*, 2880–2889. [[CrossRef](#)]
37. Qiu, J.P.; Tong, Y.W.; Zhao, D.M.; He, Z.Q.; Chen, J.M.; Song, S. Electrochemical reduction of CO₂ to methanol at TiO₂ nanotube electrodes. *Acta Phys.-Chim. Sin.* **2017**, *33*, 1411–1420.
38. Rosen, J.; Hutchings, G.S.; Lu, Q.; Rivera, S.; Zhou, Y.; Vlachos, D.G.; Jiao, F. Mechanistic insights into the electrochemical reduction of CO₂ to CO on nanostructured Ag surfaces. *ACS Catal.* **2015**, *5*, 4293–4299. [[CrossRef](#)]
39. Hsieh, Y.-C.; Senanayake, S.D.; Zhang, Y.; Xu, W.; Polyansky, D.E. Effect of chloride anions on the synthesis and enhanced catalytic activity of silver nanocoral electrodes for CO₂ electroreduction. *ACS Catal.* **2015**, *5*, 5349–5356. [[CrossRef](#)]
40. Wang, Y.; Liu, J.; Wang, Y.; Al-Enizi, A.M.; Zheng, G. Tuning of CO₂ reduction selectivity on metal electrocatalysts. *Small* **2017**, *13*, 1701809. [[CrossRef](#)]
41. Bui, L.; Chakrabarti, R.; Bhan, A. Mechanistic origins of unselective oxidation products in the conversion of propylene to acrolein on Bi₂Mo₃O₁₂. *ACS Catal.* **2016**, *6*, 6567–6580. [[CrossRef](#)]
42. Ma, M.; Trzesniewski, B.J.; Xie, J.; Smith, W.A. Selective and efficient reduction of carbon dioxide to carbon monoxide on oxide-derived nanostructured silver electrocatalysts. *Angew. Chem.-Int. Ed.* **2016**, *55*, 9748–9752. [[CrossRef](#)] [[PubMed](#)]
43. Kim, C.; Jeon, H.S.; Eom, T.; Jee, M.S.; Kim, H.; Friend, C.M.; Hwang, Y.J. Achieving selective and efficient electrocatalytic activity for CO₂ reduction using immobilized silver nanoparticles. *J. Am. Chem. Soc.* **2015**, *137*, 13844–13850. [[CrossRef](#)] [[PubMed](#)]
44. Delacourt, C.; Ridgway, P.L.; Kerr, J.B.; Newman, J. Design of an electrochemical cell making syngas (CO + H₂) from CO₂ and H₂O reduction at room temperature. *J. Electrochem. Soc.* **2008**, *155*, B42–B49. [[CrossRef](#)]
45. Yano, J.; Yamasaki, S. Pulse-mode electrochemical reduction of carbon dioxide using copper and copper oxide electrodes for selective ethylene formation. *J. Appl. Electrochem.* **2008**, *38*, 1721–1726. [[CrossRef](#)]

